Journal of Power Sources 195 (2010) 5114–5121

Contents lists available at ScienceDirect

Journal of Power Sources

journal homepage: www.elsevier.com/locate/jpowsour

Pyridinium-based protic ionic liquids as electrolytes for RuO_2 electrochemical capacitors

Laurence Mayrand-Provencher, Sixian Lin, Déborah Lazzerini, Dominic Rochefort*

Département de chimie, Université de Montréal, CP6128 Succ. Centre-Ville, Montréal, Québec, Canada H3C 3J7

ARTICLE INFO

Article history:
Received 2 February 2010
Received in revised form 22 February 2010
Accepted 23 February 2010
Available online 1 March 2010

Keywords:
Electrochemical capacitor
Pseudocapacitance
Energy-storage
Ruthenium dioxide
Room temperature molten salt
Structure–property relationships

ABSTRACT

A series of pyridinium-based room temperature protic ionic liquids has been synthesized and their key properties, including dynamic viscosity, density, ionic conductivity, glass transition temperature, and potential window on Pt and on glassy carbon have been determined. In order to evaluate the PILs performance as electrolytes in metal-oxide based electrochemical capacitor, the specific capacitance (from 40 to 50 $F\,g^{-1}$) and the specific charge (from 23 to 48 $C\,g^{-1}$) of a thermally prepared RuO_2 electrode have been measured. This class of protic ionic liquids was found to exhibit very low viscosities (from 2.77 to 87.9 cP) along with conductivities ranging from 1.10 to 11.25 $mS\,cm^{-1}$, which are properties of the highest importance for applications in energy-storage devices. Structure–property relationships, including the effect of the alkyl chain length of the cation's substituent and of its position, are reported and should improve the success of the rational design of protic ionic liquids for specific applications in the future.

1. Introduction

Electrochemical capacitors (ECs) or supercapacitors are energy-storage devices which can provide high power outputs for short periods of time. This property of ECs can be advantageously utilized in electronics [1] but one of their most promising applications is undoubtedly their use as auxiliary energy sources in hybrid and electrical vehicles by providing the power bursts necessary for acceleration and by recuperating the energy from braking [2].

ECs made from RuO_2 have been reported to yield the highest specific capacitance (C_s) so far, with values as high as 977 $F\,g^{-1}$ being obtained by Liu and Pickup [3] using hydrous RuO_2 powder electrodes prepared with a variant of the sol-gel process developed by Zheng et al. [4]. Such metal-oxide based ECs rely on a charge storage mechanism named "pseudocapacitance", which involves faradaic processes or partial faradaic transfers [5]. In RuO_2, pseudocapacitance is possible via proton-coupled reactions which imply a shift in oxidation state from Ru^{4+} to Ru^{3+} and Ru^{2+} (Eq. (1)). This process is known to be extremely reversible with a proper electrolyte, giving mirror-like cyclic voltammograms.

$$RuO_2 + \alpha H^+ + \alpha e^- \rightleftharpoons RuO_{2-\alpha}(OH)_\alpha \quad (1)$$

In most papers dedicated to RuO_2 based ECs, acidic aqueous solutions are used as electrolytes because protons are necessary for pseudocapacitance to arise on this material. Unfortunately, these electrolytes have a restrained temperature domain of utilization and a narrow potential window of stability (~1 V), limiting their scope of applications. Indeed, being able to use ECs at high temperatures is desirable to increase the electrolyte conductivity and decrease its viscosity, while a large potential window is of importance since the maximum energy stored and the maximum power delivered by ECs is related to the square of the cell voltage [2,6]. Protic ionic liquids can offer an interesting alternative to aqueous electrolytes by potentially allowing to overcome all of their inherent limitations. These fused salts are a subclass of ionic liquids (ILs) which regroups those obtained by the proton transfer from a Brønsted acid to a Brønsted base. For carefully chosen anions and cations, they provide a much larger electrochemical window of stability (e.g. up to 3 V for pyrrolidinium PILs [7]), a higher boiling point, a better thermal stability, and a higher proton content than aqueous solutions.

Recently, we showed that pseudocapacitance can arise on RuO_2 using PILs as the electrolyte [8]. The cyclic voltammograms recorded for a crystalline RuO_2 electrode in a PIL composed of 2-methylpyridine and trifluoroacetic acid possessed the distinctive features resulting from changes in the oxidation state of Ru (redox peaks). We have discussed on important relationships between the properties of various PILs and their capacitive behavior on RuO_2, including the influence of their viscosity and conductivity on the C_s obtained [9]. While most of the PILs studied had satisfying potential window of stability on RuO_2 (up to 1.5 V), their C_s determined by cyclic voltammetry was at most two thirds of

* Corresponding author. Tel.: +1 514 343 6733; fax: +1 514 343 7586.
E-mail address: dominic.rochefort@umontreal.ca (D. Rochefort).

0378-7753/$ – see front matter © 2010 Elsevier B.V. All rights reserved.
doi:10.1016/j.jpowsour.2010.02.073

that obtained in an aqueous H_2SO_4 0.1 M solution (after 10 cycles) and their high viscosities led to a significant decrease of capacitance upon cycling which did not occurred in H_2SO_4. Hence, it was concluded that PILs with enhanced properties needed to be designed in order to be applied as electrolytes in ECs with overall performances equivalent or better to those obtained with aqueous electrolytes.

The tailoring of PILs properties can be done by carefully choosing the anion and cation composing them as even small structural changes in these constituents can drastically affect the properties of the melts [10]. However, designing optimized PILs requires a thorough understanding of the structure–properties relationships and while several studies have been devoted to the determination of these relationships in series of ILs [11–20], only a few were carried out exclusively for PILs [10,21,22]. Recent results also pointed out that deep analyses of IL–metal-oxide electrodes interactions are required in order to develop task-specific ionic liquids for ECs [23–25]. Clearly, there is a need for a better understanding of how the properties of ionic liquids affect processes at an electrode and, here, we will focus on those involved at a RuO_2 electrode.

Since PILs composed of 2-methylpyridine and trifluoroacetic acid (TFA) are probably those with the most advanced physicochemical characterization and the ones that have been the most studied in the literature [8,9,23,24,26–28], we used the structure of their anion and cation as a starting point to investigate important relationships between some of their structural aspects and their properties. Hence, in this work, cations with small structural variations from 2-methylpyridinium have been investigated using trifluoroacetate as the anion. The influence of the anion was then evaluated from mixtures of 2-methylpyridine with formic acid (Fm), trifluoroacetic acid or trifluoromethanesulfonic acid (Tf). Also, in order to evaluate the PILs relative performance as electrolytes in metal-oxide based ECs, the C_s and the specific charge (Q_s) obtained on a crystalline, thermally prepared RuO_2 electrode submerged in the PILs have been measured. This type of electrodes provide much smaller capacitances than powder electrodes based on amorphous RuO_2, but while they might not be appropriate to yield high energy, high power devices, their good physical robustness and chemical stability makes them candidates of choice to make comparisons between electrolytes.

Structure–property relationships, including the effect of the alkyl chain length of the cation's substituent and of its positioning, are reported here and should improve the chances of success of the rational design of PILs with desirable properties in the future.

2. Experimental

2.1. Materials

2-Pentylpyridine (≥98%), $RuCl_3{\cdot}xH_2O$ (99.98%), oxalic acid dihydrate (99%) and Ti sheets (0.25 mm width, 99.7%) used as electrode substrate were purchased from Sigma–Aldrich. 2-Methylpyridine (>98%), 3-methylpyridine (99%), 4-methylpyridine (98%), 2-ethylpyridine 98%), 3-ethylpyridine (98%), 4-ethylpyridine 98%), 2-phenylpyridine (98%), trifluoroacetic acid (99%) and trifluoromethanesulfonic acid (>98%) were obtained from Alfa Aesar. Formic acid (∼98%) and HYDRANAL®-Coulomat AG were purchased from Fluka. Acetonitrile (>99.99%) was bought from EMD Chemicals. All reagents were used as received.

2.2. Ionic liquids synthesis

All PILs were prepared by the slow addition (1 mL min^{-1}) of the acid in its respective base at room temperature (RT = 21 ± 3 °C) and while stirring. In order to eliminate traces of water either coming from the starting materials or from the atmosphere, the resulting mixtures were heated at 70 °C for 48 h under vacuum. Sufficiently large quantity of PILs (from 35 to 150 mL) were prepared in order to obtain high-yield synthesis and to thus to ensure that the base:acid ratio was as unchanged as possible from the initial reagent proportions [28]. All PILs samples were kept sealed in vials using thick layers of paraffin sheets between uses.

2.3. Ionic conductivity

The conductivity of the PILs (σ) was measured by electrochemical impedance spectroscopy using a potentiostat from Princeton Applied Research (model PARSTAT 2273) and a low-volume Orion conductivity cell (model 018012) with two platinized electrodes. σ was calculated from the electrolyte resistance (R_s) determined as the intersection of the curve obtained with the real axis (Z_{Re}) of the Nyquist plot obtained by scanning from 10^{-1} to 10^5 Hz around open circuit potential and with a perturbation amplitude of 10.0 mV rms (see Appendix A for an example). A thermocouple was placed in direct contact with the PIL in the cell to accurately determine its temperature (±0.1 °C).

2.4. Dynamic viscosity

The kinematic viscosity (ν) was measured at 27.0 ± 0.1 °C (in triplicate) using an ASTM Kinematic Viscometer (cross-arm type, size 4). The density (ρ) was measured (in triplicate) by weighting 1.00 mL of PIL at RT. The dynamic viscosity (η) was then calculated from these measurements ($\eta = \nu\rho$).

2.5. Preparation of the thermal RuO_2 film electrode

A thin layer of $RuCl_3{\cdot}xH_2O$ solubilized in isopropanol (0.1 M) was painted on both sides of a 0.50 cm × 1.00 cm section of a Ti substrate previously etched with oxalic acid and the thermal decomposition of this solution was carried out in air (at 400 °C, for 2 h) to obtain a RuO_2 film. This procedure was repeated twice to yield a loading of 1.2 mg cm^{-2} of electroactive material (geometric area = 1 cm^2). X-ray analyses of the deposit yielded a typical diffractogram for crystalline RuO_2 [29] and SEM analyses revealed a good film uniformity (see Appendix A).

2.6. Electrochemical measurements

As described in details elsewhere [28], the electrochemical window of stability of the PILs on Pt (BAS, 0.0249 cm^2) and on glassy carbon (GC) (BAS, 0.0707 cm^2) was evaluated using an Ag wire quasi-reference electrode (AgQRE), a Pt spiral auxiliary electrode, and the PARSTAT 2273.

The capacitive behavior of the PILs was investigated using a homemade heart-shaped electrochemical cell and the thermally prepared RuO_2 electrode, which was weighted prior to any measurement in order to ensure that no mass loss of the deposit would affect the specific capacitance and specific charge data. An Ag/AgCl reference electrode (3 M KCl) was used in aqueous H_2SO_4 solutions and an AgQRE was used for measurements in ILs in order to avoid electrolyte contamination by water. A spiral of Pt wire was used as the auxiliary electrode. The RuO_2 electrode was cleansed electrochemically with 20 cycles in H_2SO_4 0.1 M from 0 to 1 V at 50 mV s^{-1} and then rinsed with water and acetone prior to each analysis in the PILs. The electrolytes were degassed for at least 15 min with nitrogen and the working electrode was submerged with the degassed liquids for 5 min before any measurements were made. All measurements were carried out at RT.

2.7. Glass transition temperature

The PILs' glass transition temperatures were measured using a differential scanning calorimeter from TA Instruments (model Q2000). Hermetic Al pans and hermetic Al lids were bought from Instrument Specialists Inc. and were used for all measurements. Samples were cooled from 40 to −150 °C at 10 °C min^{-1} and they were held at that temperature for 5 min. They were then heated at the same rate from −150 °C until the T_g was observed. The T_g was defined as the temperature corresponding to half of the glass transition of the heating curve.

2.8. Chemical purity

The purity of all neat PILs was determined by ^{1}H NMR spectroscopy using a 300 MHz instrument (model Bruker Avance 300) and a coaxial tube set purchased from Wilmad Labglass (Inner tube outer diameter = 2.97 mm; inner diameter = 1.96 mm). $CDCl_3$ was used as an external lock. Clean spectra (not shown) were obtained in all cases in which all peaks are ascribable to the PILs' constituents.

2.9. Optical purity

The absorption profile of the PILs was determined by scanning from 190 to 1100 nm by UV–vis spectroscopy while using 1 cm quartz cells and a spectrophotometer from Thermo Instruments (model Nicolet Evolution 100). The samples to analyze were prepared by diluting 100 μL of the PILs in 900 μL of acetonitrile, which was also the blank for these experiments.

2.10. Water content

The amount of water contained in the PILs was determined using a coulometric Karl-Fisher titrator from Mettler Toledo (model C30) and HYDRANAL®-Coulomat AG as the reagent. 0.4 mL samples of PILs were injected in the titrator while using a syringe washed beforehand with the sample to analyze. Since the water content of the PILs was found to increase as the liquids were manipulated and exposed to the atmosphere, it must be specified that the values reported in this work were collected shortly after measuring the physicochemical properties but prior to the electrochemical data acquisition.

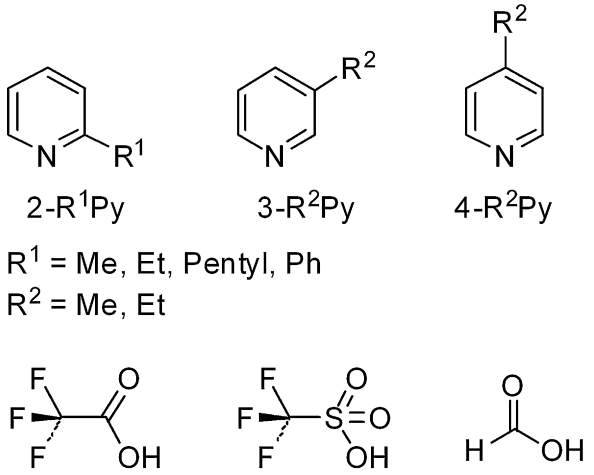

Fig. 1. Structure of the bases and acids used given with their corresponding abbreviation (Py = pyridine, TFA = trifluoroacetic acid, Tf = trifluromethanesulfonic acid, Fm = formic acid).

3. Results and discussion

3.1. Physicochemical properties and phase transitions of the PILs

In this work, pyridinium-based PILs with the constituents shown in Fig. 1 have been synthesized and the notation described in Fig. 1 will henceforth be used. In addition to the 1:1 base to acid molar ratio (the term base:acid ratio will be employed) which is a reagent proportion commonly used to make ILs, the 1:2 base:acid ratio has been studied since it yields PILs of different properties and that, similarly to what has been observed by Angell and co-workers with mixtures made from 2-MePy and TFA in different proportions [26], a maximum boiling points should be obtained at the 1:2 ratio due to the formation of the dimer $[(CF_3CO_2)_2H]^-$ for the melts with TFA as the acid. Also, even if it is believed that Fm and Tf do not form dimers at the 1:2 ratio, these mixtures have been studied for comparison purposes. The effect of the constituents' proportion is clearly seen in Table 1 in which the physicochemical properties of the PILs of both ratios are reported. Similarly to what has been observed for other heterocyclic amine based PILs using TFA as the

Table 1
Physicochemical properties of the studied liquids and electrochemical data obtained by CV while using them as electrolytes with a thermally prepared RuO_2 electrode.

Electrolyte	$\eta \pm$ CI (95%) (27.0 °C) (cP)	$\rho \pm$ CI (95%) (RT) (g mL^{-1})	$\sigma \pm \Delta\sigma$[a] (27.0 °C) (mS cm^{-1})	$E_{a\sigma}$ (kJ mol^{-1})	C_s (RT) (F g^{-1})	Q_s (RT) (C g^{-1})
2-MePy:TFA (1:1)[b]	25.05 ± 0.17	1.318 ± 0.008	3.39 ± 0.02	25.1	44	41
2-MePy:TFA (1:2)[b]	13.12 ± 0.03	1.402 ± 0.002	9.25 ± 0.05	17.3	44	42
2-EtPy:TFA (1:1)	20.27 ± 0.64	1.247 ± 0.015	3.13 ± 0.03	23.0	49	47
2-EtPy:TFA (1:2)	13.77 ± 0.25	1.380 ± 0.023	8.25 ± 0.02	16.9	50	48
2-PentylPy:TFA (1:1)	33.87 ± 0.36	1.167 ± 0.008	1.10 ± 0.01	27.4	40	38
2-PentylPy:TFA (1:2)	19.89 ± 0.19	1.235 ± 0.028	3.39 ± 0.03	19.9	44	43
2-PhPy:TFA (1:2)	87.9 ± 1.6	1.378 ± 0.021	1.339 ± 0.003	18.2	40	40
3-MePy:TFA (1:2)	14.94 ± 0.07	1.396 ± 0.006	9.35 ± 0.10	20.0	42	40
3-EtPy:TFA (1:1)	22.62 ± 0.35	1.252 ± 0.019	3.87 ± 0.04	26.0	46	35
3-EtPy:TFA (1:2)	14.60 ± 0.43	1.358 ± 0.024	8.27 ± 0.09	19.2	43	41
4-MePy:TFA (1:2)	15.55 ± 0.07	1.401 ± 0.006	8.28 ± 0.09	20.3	43	41
4-EtPy:TFA (1:2)	13.57 ± 0.30	1.329 ± 0.027	7.61 ± 0.08	19.2	41	38
2-MePy:Tf (1:2)	16.93 ± 0.10	1.561 ± 0.007	11.25 ± 0.06	16.5	43	47
2-MePy:Fm (1:1)	2.77 ± 0.04	1.048 ± 0.009	n.d.[c]	n.d.[c]	46	23
2-MePy:Fm (1:2)	6.20 ± 0.25	1.131 ± 0.010	n.d.[c]	n.d.[c]	47	23
H_2SO_4 0.1 M (aq)[d]	0.8328 ± 0.02	0.996 ± 0.005	46.04 ± 0.35	n.d.	61	61

[a] The accuracy of σ ($\Delta\sigma$) was calculated using the relation $\Delta\sigma = \sigma\,[(\Delta K/K)^2 + (\Delta R_s/R_s)^2]^{1/2}$, where K is the cell constant of the conductivity cell, where R_s is the electrolyte resistance and where ΔK and ΔR_s are their confidence interval (CI) at 95% (n = 3). Data from the measurements with the KCl standard solution are used as an estimate of the ΔR_s.

[b] η, ρ and σ were determined in Ref. [28].

[c] Bubbles formed at the platinized electrodes surface upon filling the conductivity cell with PIL.

[d] η and σ were determined in Ref. [9].

Table 2
Water content, glass transition temperature, electrochemical stability, and miscellaneous data for the studied PILs.

Electrolyte	Water content (wt.%)	T_g (°C)	Electrochemical window		Upper potential limit on RuO_2 (V vs. AgQRE)	ΔpK_a[a]	Total yield (%)
			On Pt (V vs. AgQRE)	On GC (V vs. AgQRE)			
2-MePy:TFA (1:1)	0.29	−87	−0.4 to 2.0	−1.2 to 1.8	1.4	5.42	99.0
2-MePy:TFA (1:2)	0.11	−95	−0.4 to 2.1	−1.4 to 1.6	1.4	5.42	99.3
2-EtPy:TFA (1:1)	0.91	−90	−0.3 to 2.0	−1.0 to 1.8	1.4	5.36	91.2
2-EtPy:TFA (1:2)	0.07	None[b]	−0.6 to 2.0	−0.8 to 1.5	1.4	5.36	99.1
2-PentylPy:TFA (1:1)	0.54	−83	−0.3 to 2.1	−0.7 to 1.9	1.4	5.48	98.1
2-PentylPy:TFA (1:2)	0.09	−93	−0.2 to 2.1	−0.5 to 1.7	1.4	5.48	96.3
2-PhPy:TFA (1:2)	0.08	−62	−0.3 to 1.6	−1.0 to 1.7	1.4	3.91	98.2
3-MePy:TFA (1:2)	0.19	−94	−0.5 to 2.0	−1.2 to 1.7	1.2	4.99	98.3
3-EtPy:TFA (1:1)	0.54	None[b]	−0.5 to 2.0	−1.0 to 2.5	1.2	5.05	96.7
3-EtPy:TFA (1:2)	0.17	−97	−0.4 to 2.0	−0.9 to 1.7	1.2	5.05	94.9
4-MePy:TFA (1:2)	0.12	−91	−0.5 to 2.0	−1.5 to 1.6	1.4	5.41	97.2
4-EtPy:TFA (1:2)	0.05	−94	−0.5 to 2.0	−1.5 to 1.7	1.1	5.55	97.5
2-MePy:Tf (1:2)	0.30	−100	−0.3 to 2.2	−1.3 to 2.2	1.6	∼20	97.2
2-MePy:Fm (1:1)	0.45	−114	None	−1.0 to 1.2	0.6	2.21	98.8
2-MePy:Fm (1:2)	0.76	−105	None	−1.0 to 1.2	0.6	2.21	98.1

[a] pK_a in water obtained from the calculated properties of the SciFinder Scholar™ 2006 database using the Advanced Chemistry Development Software V8.14 for Solaris. pK_a reported for TFA and Fm are 0.53 and 3.74, respectively.
[b] No T_g was observed for this PIL by DSC at a scanning rate of 10 °C min^{-1}.

acid [9], higher conductivities are obtained at the 1:2 ratio which could be explained by the generally smaller viscosities of the mixtures at this composition. Achieving high ionic conductivities and low viscosities is of major importance for PILs-based electrolytes in energy-storage devices, hence justifying our investigations on PILs at 1:2 base:acid ratio.

The PILs obtained in this work present color ranging from pale yellow to dark brown, indicating that they contain colored impurities since most pure PILs are colorless. However, despite of the darker coloration of heated PILs which resulted in absorption profiles of greater magnitudes, their physicochemical properties of interest were found to be identical to those obtained before their heating step, which shows that the presence of such impurities has no effect on their properties (explained in details elsewhere [28]). The PILs were therefore used without any further purification. However, the properties of 2-EtPy:TFA (1:1) were significantly altered during the heating step and the small yield of its synthesis (91.2%) suggests a change in its base:acid ratio. All other PILs were obtained with high yields (see Table 2 in which the yields are reported in wt.% of the initial amount of reagent used) indicating that their final base:acid ratio is representative of the initial reagent molar proportions. The water contents of the PILs are also reported in Table 2 and they are within the same range of what is typically reported in the literature [30].

Only the PILs with a melting point below RT have been extensively characterized and no data are reported for 3-MePy:TFA (1:1), 4-MePy:TFA (1:1), 4-EtPy:TFA (1:1) and 2-PhPy:TFA (1:1) which gave solids with melting points (measured in an open capillary) of respectively 37, 110, 84 and 45 °C. Also, a portion of 2-MePy:Tf (1:1) crystallized at room temperature which is why it has not been characterized either. The high melting point of 4-MePy:TFA (1:1) has been attributed to the axis of symmetry of its cation which increase its packing efficiency [30]. In comparison, the lower melting point of 4-EtPy:TFA (1:1) reflects the asymmetry introduced by its ethyl group and its higher mobility than the methyl.

The strong ion–ion interactions due to the large ΔpK_a of 2-MePy:Tf (1:1) (∼20) are most likely responsible of its crystallization at RT. The ΔpK_a, defined as the pK_a difference between the base and acid in water, is linked to the probability of reforming the neutral species. Hence, a large ΔpK_a indicates a strong proton transfer and a good ionicity. On the other hand, if the ΔpK_a is small, a poor ionicity is obtained and important losses of the neutral species can occur by volatilization during the heating step. This can leads to alterations of the PILs' base:acid ratio and, therefore, in order to minimize this effect and to obtain PILs of sufficient ionicities, the bases in this work were selected deliberately in order to have a sufficiently large ΔpK_a with TFA.

In addition to the approximation provided by the ΔpK_a, the ionicity of the PILs can be estimated qualitatively from the region in which they are located on a Walden plot [31]. This type of plots corresponds to the log of the ILs equivalent conductivity (Λ) as a function of the log of their fluidity (η^{-1}) and the ideal line it contains is described by a diluted KCl aqueous solution which has ions that are fully dissociated and of an equivalent mobility (see Fig. 2). ILs of a "good" quality will appear near or over this ideal line and such ILs should be of a greater ionicity than those termed of "poor" quality which appear well below that line. The "poor" and "good" qualifications used in this work are based on a classification proposed by Angell and co-workers [32]. Fig. 2 shows that all the PILs studied here are under this ideal line and can therefore be considered of a poor quality. This is typical for protic ionic liquids because an equilibrium exists between their ionic and neutral species which reduces the effective number of charge carriers that they contain. Consequently, the higher ionicity obtained for

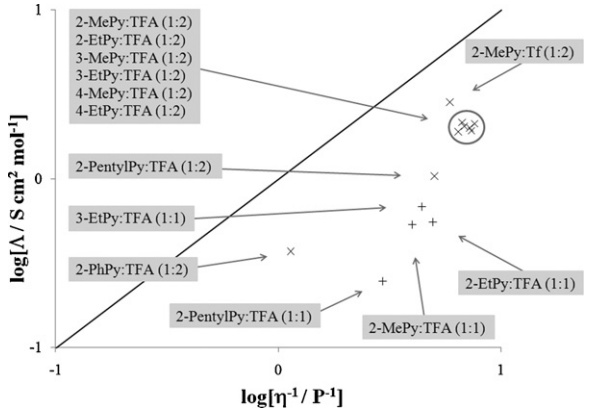

Fig. 2. Walden plot for the studied PILs obtained from the conductivity and viscosity measured at 27.0 °C. The ideal line is given by a 1 M KCl aqueous solution in which the behavior of independent ions is followed. The "+" and "×" represents respectively PILs of the 1:1 and 1:2 base:acid ratios.

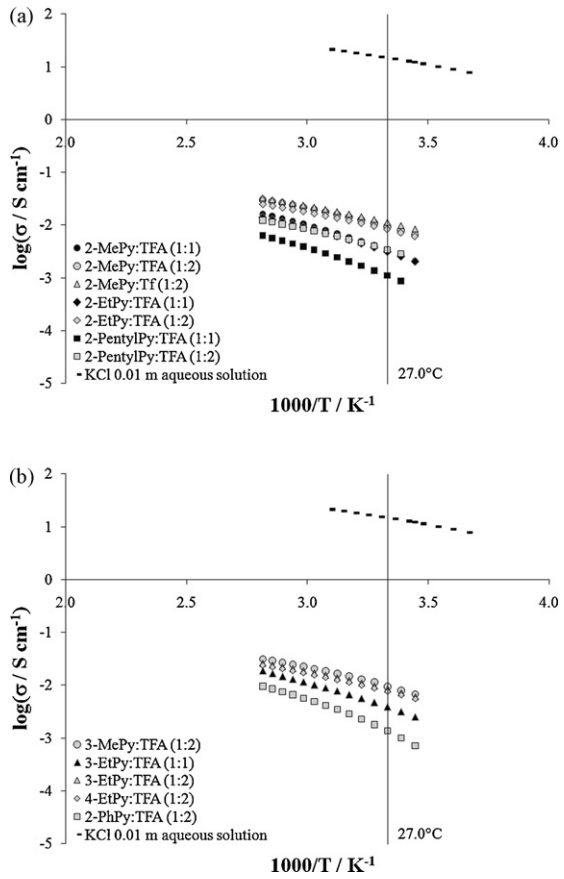

Fig. 3. Arrhenius plots for the PILs and a KCl 0.01 m aqueous solution. The data for the KCl solution were obtained from the literature [34]. Measurements were done at an interval of 5 °C from 17 to 82 °C. The R^2's obtained for the fittings ranged from 0.9881 to 0.9970.

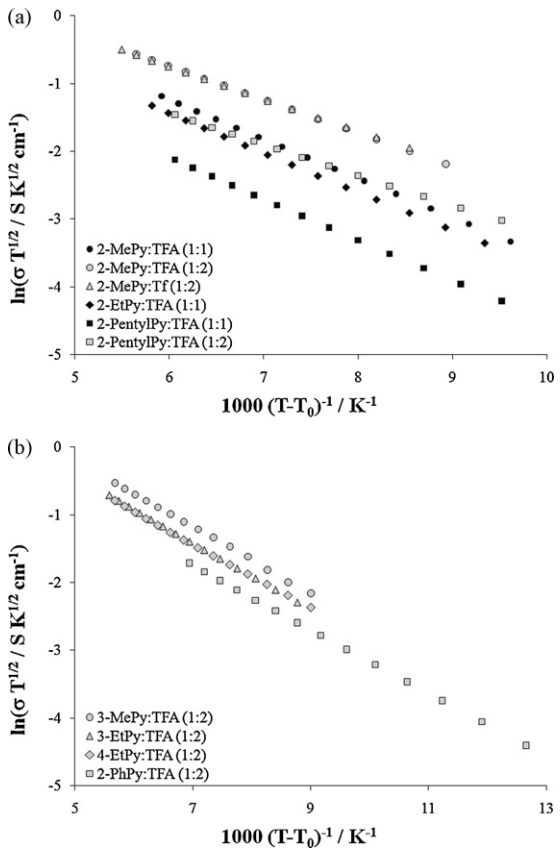

Fig. 4. VTF plots obtained for the studied PILs. The R^2's obtained for the fittings were greater or equal than 0.9994 in all cases.

2-MePy:Tf (1:2) ($\Delta pK_a \approx 20$) results in a point lying closer to the line. Also, the fact that they lie under the ideal line indicates that the PILs' conductivity mechanism is predominantly of the vehicle-type [9]. The PILs with a 1:2 base:acid ratio reported here lie closer to the ideal line and have a greater equivalent conductivity for an equal or greater fluidity than their corresponding 1:1 PILs, which indicates that they present a better ionic character that can only be obtained if the second equivalent of TFA participate in the proton exchange process.

The temperature affects the conductivity of ILs in relation to the ion–ion interactions between the charge carriers that they contain. In protic ILs, hydrogen bonds are another important type of interaction which can play a role in the dependence obtained with the temperature. Fig. 3 illustrates this dependence of the PILs' conductivities with their temperature in the common Arrhenius form. At high temperatures, the Arrhenius equation provides a good fitting with the behavior obtained and linear relationships are observed. The slopes of the trend lines obtained with the data in this region of the plot are used to calculate the activation energy for the conductivity of the PILs ($E_{a\sigma}$) and these values are reported in Table 1. The smaller $E_{a\sigma}$ obtained for the 1:2 base:acid ratio reflects the different temperature dependence of those PILs and the weaker interactions between their constituents, which is consistent with the smaller T_g values obtained for these 1:2 melts in comparison to 1:1 (Table 2). Indeed, the T_g is also an indication of the cohesive energy within the PILs, smaller T_g values being associated with weaker coulombic and van der Waals interactions [32].

The curvature obtained at lower temperatures shows that a faster decrease rate than predicted by the Arrhenius relationship is obtained for the conductivity with temperature and this typical behavior is due to changes in the transport properties of the PILs [32]. The empirical Vogel–Tamman–Fulcher (VTF) equation is an alternative way of representing the behavior of σ vs. T and it provides better fits for such systems that can vitrify. Eq. (2) shows this VTF equation where A and B are constants and where T_0 is the ideal glass transition temperature (the approximation $T_0 = T_g$ is used). Fig. 4 shows that a better linearity is obtained with this equation which is confirmed by the R^2's calculated from the data of the PILs which are nearer of unity ($R^2 \geq 0.9994$) than those calculated from the Arrhenius plots shown in Fig. 3 ($0.9881 \leq R^2 \leq 0.9970$). This is yet another indication of the presence of strong interactions between the charge carriers within the PILs.

$$\sigma = \frac{A}{\sqrt{T}} \exp\left(\frac{-B}{T - T_0}\right) \quad (2)$$

Another important factor upon which the conductivity is dependant is the viscosity of the melts. An important inverse correlation exists between the two and this can be seen from the data in Table 1 where highly conductive PILs also have low viscosities. The pyridinium PILs reported in this work exhibit low viscosities in comparison to most other classes of PILs [30]. However, 2-PhPy:TFA (1:2) stands out with its high viscosity (87.9 cP at 27.0 °C) and this would be explained by the additional intermolecular interactions due to the larger size of the cation and to π–π stacking between the phenyls.

The density is another key property of PILs that is used to calculate their dynamic viscosity but that can also be related to their conductivity. Table 1 shows that, for both the 1:1 and 1:2 ratios and for all of the three positions studied (2-, 3-, 4-), the density decreases as the alkyl chain length of the cation's substituent increases. Similar results have also been reported elsewhere for

aliphatic quaternary ammonium ILs with perfluoroalkyltrifluoroborates [16] and for PILs with alkylammonium cations [10] and this can be attributed to the greater steric hindrance of cations with longer, bulkier chains. Besides, because of their smaller density and of the greater molecular weight of their cation, PILs that have cations with substituents of longer chain length possess a lesser amount of charge carriers per unit of volume, which contributes to their smaller ionic conductivities. Again, independently of the substituent's positioning and of the base:acid ratio, the conductivities shown in Table 1 are smaller for longer alkyl chains.

Longer alkyl chain length for the cation's substituent can be expected to increase the viscosity obtained for the PILs because of the greater amount of van der Waals interactions and this behavior has been reported previously for PILs with alkylammonium cations [10] and for many aprotic ionic liquids [14,18], a subclass of ILs which excludes PILs. In this work, PILs with the longest alkyl substituent (Pentyl) have the highest viscosities (for both base:acid ratios) which is consistent with this trend. However, the dependency of viscosity upon the chain length for shorter alkyl substituent is more complex. By comparing PILs with the same ratio and substituent's position among themselves, the viscosity obtained with an ethyl group was found to be either smaller, equal, or larger than with a methyl. The explanation behind the smaller viscosities obtained with ethyl groups is unclear, but similar phenomena have been obtained with other types of PILs [21] and we can hypothesize that, in some cases, the higher mobility of the ethyl group can be the dominant effect over the increase in van der Waals forces due to its longer chain than the methyl.

The effect of the anionic component on the physicochemical properties of the melts can be seen in Table 1 where the viscosities obtained for the PILs with the 2-MePy cation follow the trend Fm < TFA < Tf. The highest conductivity is also obtained with triflate anion, in agreement with similar results reported previously [26].

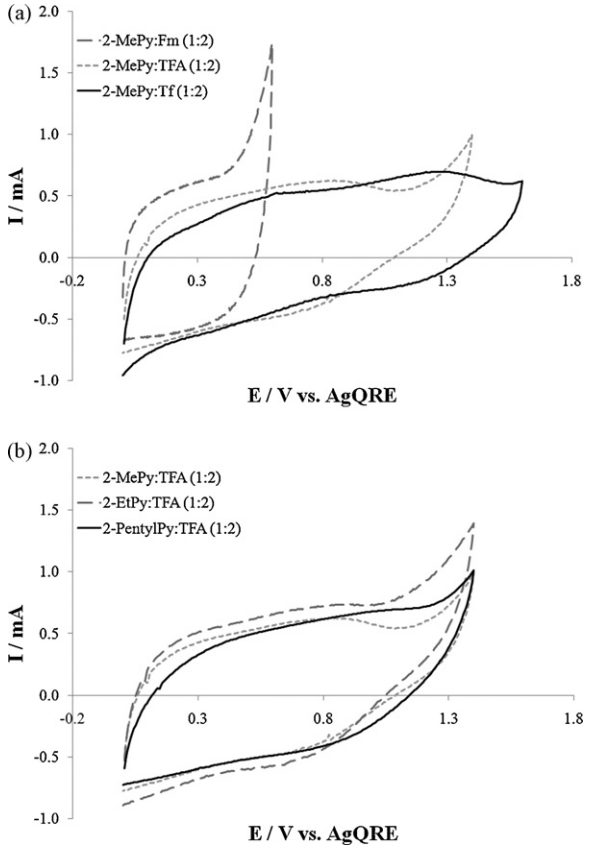

Fig. 5. (a) Effect of the anion used and (b) effect of the cations alkyl chain length on the cyclic voltammograms obtained for various PILs. All data are given for the 20th cycle gathered at 10 mV s^{-1} using the same thermally prepared RuO_2 electrode with a loading of 1.2 mg cm^{-2} (geometric area = 1 cm^2).

3.2. Pseudocapacitive behavior of RuO_2 in PILs

We then evaluated the performance of these electrolytes for applications in metal-oxide based electrochemical capacitors. The specific capacitance (C_s) and the specific charge (Q_s) of a RuO_2 electrode were determined by cycling voltammetry (scan rate of 10 mV s^{-1}) from integrating the area under the curve of the 20th scan from 0.8 to 0.2 V in the cathodic current section.

C_s values are useful to compare the energy stored by RuO_2 in various electrolytes, but Q_s can provide additional information for electrolytes with different electrochemical window of stability like the PILs in this work. This potential window was used for the cycling which led to the determination of C_s and Q_s and it was carefully chosen in order to avoid the strong current increase which is obtained when exceeding either the cathodic or anodic potential of electrochemical stability of the system. Exceeding these potential limits was found to alter severely the reversibility and the shape of the CV curves along with both the C_s and Q_s values calculated due to electrolyte oxidation and H_2 evolution.

The reversibility of the redox phenomena involved can be judged by the comparison between the cathodic and anodic currents. In H_2SO_4 0.1 M aqueous solutions, this reversibility of the proton-coupled charge transfer with RuO_2 is very good and a sharp inversion of the current from positive to negative values is observed [9], yielding voltammograms of a rectangular shape. However, for more viscous media, a slow current diminution is obtained after inversing polarity which results in curves of less mirror-like shapes. Fig. 5 shows examples of CV curves obtained in which the high viscosity of the PILs is clearly reflected by this slow current inversion. In Fig. 5, CV curves with high currents values typical of pseudocapacitance are obtained and the voltammogram of 2-MePy:Tf (1:2) in Fig. 5a clearly exhibits the redox peaks attributable to shift of oxidation state in RuO_2. Fig. 5a also demonstrates that the choice of the anion used affects greatly the shape of the voltammograms obtained. However, the C_s reported for the PILs with the different anions (Table 1) are very similar, which indicates that currents of the same magnitude are generated within the potential domain used for the C_s calculation. Fig. 5a shows that the choice of the anion affects the upper potential limit (Fm < TFA < Tf) and, because of the restrained potential window of stability on RuO_2 of PILs with Fm as the acid, their C_s have been determined by integrating from 0.4 to 0.2 V, which corresponds to a flat current section for these PILs. The smaller width of the electrochemical window of stability of these PILs on their performance as electrolyte is clearly reflected in their Q_s values (Table 1), which are much smaller than with the other anions.

The potential domain chosen for the cycling stability with all other PILs on RuO_2 ranged between 1.1 and 1.6 V (see Table 2 for the upper potential limit). These values are narrow in comparison to those of most aprotic ionic liquids in the literature, but they are typical for PILs since the cycling is often limited cathodically by the reduction of their protons in H_2 (0.0 V vs. AgQRE was used as the lower potential limit in this work to avoid hydrogen evolution reaction). The electrochemical windows of stability of the PILs on Pt and GC have also been determined (Table 2) and an example of CV curve used to obtain these data is shown elsewhere [28]. Pt, which is a better catalyst for the reduction of protons, had higher cathodic potential limits than GC in all cases.

The strong increase in currents which restricts anodically the usage of PILs is not yet fully understood, but the maximal upper potential that can be used on RuO_2 for the cycling (Table 2) seems to be associated to structural aspects of the PILs. The effect of the

anion on this potential limit has already been discussed, but other trends were also observed. The position of the cation's substituent was found to affect this limit, the PILs with alkyl chains of various length or a phenyl at the 2- position of the cation being more anodically stable (1.4 V vs. AgQRE) than those with a substituent at the 3- position (1.2 V vs. AgQRE). Also, the base:acid ratio of the PILs did not affect this potential limit on RuO_2, which is coherent with previous studies in similar systems with *N*-heterocyclic bases and TFA [9].

The C_s and the Q_s that were obtained at 10 mV s^{-1} for the PILs in this work ranged respectively from 40 to 50 F g^{-1} and from 23 to 48 C g^{-1}. These values are too high to be accounted for only by double layer charging which shows that pseudocapacitance is involved here. This is also confirmed by previously reported results with aprotic ILs which gave C_s limited to 6.5 F g^{-1} with RuO_2, indicating the necessity of protons for pseudocapacitance to arise on this material [8,9]. In addition, the shape of the CVs and the redox peaks that were sometime observed for the PILs in this work are strong indicative of the presence of pseudocapacitance. A series of papers by Chang et al. presented the study of the pseudocapacitive behavior of MnO_2 electrode in aprotic ionic liquids [23–25]. They provided strong evidence that redox transitions occurred at the electrode in the absence of proton, which is not the case with RuO_2. Manganese dioxide undergoes redox transitions in neutral aqueous solutions with the ions acting in the material to balance the charges upon oxidation and reduction of the material. The existence of a different charge storage mechanism for RuO_2 and MnO_2 is yet another illustration of the need to develop task-specific ionic liquids that will present the required properties for a given system. Nevertheless, the C_s and Q_s values obtained for RuO_2 in PILs are smaller in comparison to the 61 F g^{-1} and 61 C g^{-1} achieved in 0.1 M H_2SO_4 electrolyte. The higher values obtained for the latter originate from its smaller viscosity, its good conductivity and the fast proton transport rate due to its Grotthus conductivity mechanism.

Despite of the different properties between the PILs of a 1:1 and 1:2 base:acid ratios, the CV curves obtained on RuO_2 were similar, yielding analogous capacitance values. No linear correlations exist between the properties of the studied PILs and either C_s or Q_s, but some general trend have been observed: the two PILs with the smallest conductivities are also those with the smallest C_s and the PILs with a smaller upper potential limit on RuO_2 usually have smaller Q_s values.

The cation's substituent alkyl chain length had little impact on the shape of the voltammogram obtained while scanning at 10 mV s^{-1} as shown in Fig. 5b. Both the C_s (44–50 F g^{-1}) and Q_s (42–48 C g^{-1}) calculated for these three PILs of different properties are comparable, indicating that, at this slow scan rate, the different physicochemical properties of these melts have only a small effect on their pseudocapacitive behavior obtained on RuO_2. Also, 2-PhPy:TFA (1:2) presented very close C_s and Q_s values to those of the PILs in Fig. 5b despite its higher viscosity and lower conductivity. No direct relationships were found between C_s or Q_s and the cation's substituent position.

To make further comparisons between the performances of the PILs for applications as electrolytes in ECs, the following experiment at different scan rates was carried on. First, prior to the measurements for a given PIL, the preparative procedure described in Section 2.6 was followed. Then, to ensure that the comparisons between the capacitances obtained at different scan rates were unaffected by the sharp decrease in capacitance observed for the first few cycles in the PILs [9], 20 cycles were gathered from 0.0 to 0.8 V at 10 mV s^{-1}. Then, three cycles were gathered at several scan rates (1, 2, 3, 5, 8, 10, 20, 50, 100 and 200 mV s^{-1}, in this respective order). The results shown in Fig. 6 demonstrate that the specific capacitance was found to decrease significantly as the scan rate is increased. This dependence on the sweeping rate of the amount of

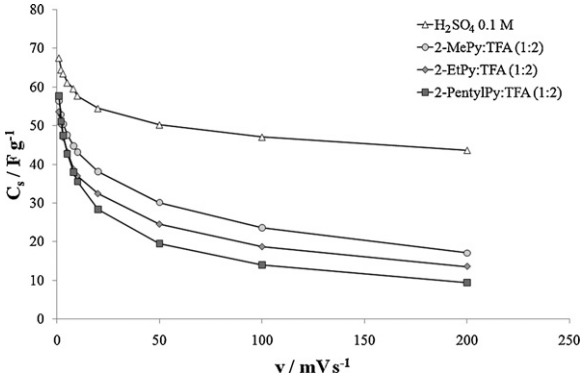

Fig. 6. Capacitance as a function of sweep rate obtained on the RuO_2 thermal electrode for H_2SO_4 0.1 M and for PILs having cations of substituents with different alkyl chain length. The C_s were calculated from the negative current section of the voltammograms from 0.6 to 0.2 V (3rd scan). The small variations in the C_s obtained at 10 mV s^{-1} in comparison to those reported in Table 1 are attributed to the different data acquisition conditions.

charges stored with thermally prepared RuO_2 electrodes is related to the existence of regions that are less accessible to react and that are thus progressively excluded as the sweep rate is increased [33]. In Fig. 6, this behavior is of a greater importance for PILs with cations having longer alkyl chain lengths. The larger viscosities and the smaller conductivities of these PILs certainly play an important role in the faster decrease observed for their capacitance since they directly influence the rate at which protons will diffuse to the active electrode material. In highly viscous electrolytes, the inner, less accessible regions of the electrode material will only be able to participate to the energy-storage processes if a sufficiently long time is provided, explaining the losses in specific capacitance observed at higher scan rates for 2-Pentyl:Py:TFA (1:2). As expected, a smaller effect of scan rate on specific capacitance is obtained with the 0.1 M H_2SO_4 aqueous electrolyte (Fig. 6) which has a very low viscosity and high proton mobility. These results clearly demonstrate that PILs with low viscosities and good conductivities are advantageous to attain high capacitance values for applications in ECs in which a fast discharge rate is necessary.

4. Conclusions

The properties of interest for pyridinium-based PILs have been determined and the viscosities of this class of PILs were found to be in the lower bracket of those typically reported in the literature. Also, the PILs of a 1:2 base:acid ratio studied had better conductivities, generally smaller viscosities and similar C_s than those of the 1:1 base acid ratio. PILs with substituents at the 2– position were found to have a slightly larger potential domain of stability for cycling on RuO_2 than those at the 3– which resulted in smaller Q_s for the latter, but the C_s were found to be comparable for all three positions of a given substituent.

PILs of a given ratio with shorter alkyl chain length for the cation's substituent were found to have higher conductivities and densities for all of the three positions studied (2-, 3-, 4-). In addition, the decrease of C_s obtained on RuO_2 as the scan rate is increased in these electrolytes shows that the viscosity and the conductivity strongly affect C_s at high scan rates.

A better understanding of such structure–properties relationships will be required to improve the rational design of PILs with specific properties to be applied as electrolytes in electrochemical capacitors. The electrochemical behavior of PILs with RuO_2 electrodes of different morphology and crystallinity as well as with other metal oxides is currently under investigation with the aim of reaching this goal.

Acknowledgements

We thank Éric Duchesne and Dr. Thierry Marris for the SEM and X-Ray analyses. This work was supported financially by a Natural Sciences and Engineering Council of Canada (NSERC) Discovery Grant. LMP acknowledges Fonds de recherche sur la nature et les technologies for a Masters Research Scholarship. SL also acknowledges NSERC for an Undergraduate Student Research Award.

Appendix A. Supplementary data

Supplementary data associated with this article can be found, in the online version, at doi:10.1016/j.jpowsour.2010.02.073.

References

[1] R.A. Huggins, Solid State Ionics 134 (2000) 179–195.
[2] R. Kötz, M. Carlen, Electrochim. Acta 45 (2000) 2483–2498.
[3] X. Liu, P.G. Pickup, J. Power Sources 176 (2008) 410–416.
[4] J.P. Zheng, P.J. Cygan, T.R. Jow, J. Electrochem. Soc. 142 (1995) 2699–2703.
[5] B.E. Conway, V. Birss, J. Wojtowicz, J. Power Sources 66 (1997) 1–14.
[6] B.E. Conway, Electrochemical Supercapacitors: Scientific Fundamentals and Technological Applications, Kluwer Academic/Plenum Publishers, New York, 1999.
[7] M. Anouti, M. Caillon-Caravanier, Y. Dridi, H. Galiano, D. Lemordant, J. Phys. Chem. B 112 (2008) 13335–13343.
[8] D. Rochefort, A.-L. Pont, Electrochem. Commun. 8 (2006) 1539–1543.
[9] L. Mayrand-Provencher, D. Rochefort, J. Phys. Chem. C 113 (2009) 1632–1639.
[10] T.L. Greaves, A. Weerawardena, C. Fong, I. Krodkiewska, C.J. Drummond, J. Phys. Chem. B 110 (2006) 22479–22487.
[11] H. Tokuda, K. Hayamizu, K. Ishii, M.A.B.H. Susan, M. Watanabe, J. Phys. Chem. B 108 (2004) 16593–16600.
[12] H. Tokuda, K. Hayamizu, K. Ishii, M.A.B.H. Susan, M. Watanabe, J. Phys. Chem. B 109 (2005) 6103–6110.
[13] R.E. Del Sesto, C. Corley, A. Robertson, J.S. Wilkes, J. Organomet. Chem. 690 (2005) 2536–2542.
[14] J.G. Huddleston, A.E. Visser, W.M. Reichert, H.D. Willauer, G.A. Broker, R.D. Rogers, Green Chem. 3 (2001) 156–164.
[15] Z.-B. Zhou, H. Matsumoto, K. Tatsumi, Chem. Eur. J. 10 (2004) 6581–6591.
[16] Z.-B. Zhou, H. Matsumoto, K. Tatsumi, Chem. Eur. J. 11 (2005) 752–766.
[17] A. Bagno, C. Butts, C. Chiappe, F. D'Amico, J.C.D. Lord, D. Pieraccinic, F. Rastrellib, Org. Biomol. Chem. 3 (2005) 1624–1630.
[18] P. Bonhôte, A.-P. Dias, N. Papageorgiou, K. Kalyanasundaram, M. Grätzel, Inorg. Chem. 35 (1996) 1168–1178.
[19] S. Busia, M. Lahtinena, H. Mansikkamäki, J. Valkonena, K. Rissanen, J. Solid State Chem. 178 (2005) 1722–1737.
[20] J.M. Crosthwaite, M.J. Muldoon, J.K. Dixon, J.L. Anderson, J.F. Brennecke, J. Chem. Thermodyn. 37 (2005) 559–568.
[21] H. Ohno, M. Yoshizawa, Solid State Ionics 154–155 (2002) 303–309.
[22] M. Hirao, H. Sugimoto, H. Ohno, J. Electrochem. Soc. 147 (2000) 4168–4172.
[23] J.-K. Chang, M.-T. Lee, C.-W. Cheng, W.-T. Tsai, M.-J. Deng, Y.-C. Hsieh, I.-W. Sun, J. Mater. Chem. 19 (2009) 3732–3738.
[24] J.-K. Chang, M.-T. Lee, C.-W. Cheng, W.-T. Tsai, M.-J. Deng, I.-W. Sun, Electrochem. Solid-State Lett. 12 (2009) A19–A22.
[25] M.-T. Lee, W.-T. Tsai, M.-J. Deng, H.-F. Cheng, I.-W. Sun, J.-K. Chang, J. Power Sources 195 (2010) 264–271.
[26] M. Yoshizawa, W. Xu, C.A. Angell, J. Am. Chem. Soc. 125 (2003) 15411–15419.
[27] Z. Duan, Y. Gu, J. Zhang, L. Zhu, Y. Deng, J. Mol. Catal. A: Chem. 250 (2006) 163–168.
[28] L. Mayrand-Provencher, D. Rochefort, Electrochim. Acta 54 (2009) 7422–7428.
[29] J.P. Zheng, T.R. Jow, J. Electrochem. Soc. 142 (1995) L6–L8.
[30] T.L. Greaves, C.J. Drummond, Chem. Rev. 108 (2008) 206–237.
[31] C. Zhao, G. Burrell, A.A.J. Torriero, F. Separovic, N.F. Dunlop, M.D.R., A.M. Bond, J. Phys. Chem. B 112 (2008) 6923–6936.
[32] W. Xu, E.I. Cooper, C.A. Angell, J. Phys. Chem. B 107 (2003) 6170–6178.
[33] S. Ardizzone, G. Fregonara, S. Trasatti, Electrochim. Acta 35 (1990) 263–267.
[34] D.R. Lide, CRC Handbook of Chemistry and Physics, 86th ed., CRC Press, New York, 2005.